NOTES AND CORRESPONDENCE

Resolution Dependence of the Tropopause Inversion Layer in an Idealized Model for Upper-Tropospheric Anticyclones

ANDREAS MÜLLER AND VOLKMAR WIRTH

University of Mainz, Mainz, Germany

(Manuscript received 18 February 2009, in final form 4 May 2009)

ABSTRACT

This note investigates the dependence of the extratropical tropopause inversion layer (TIL) on numerical resolution in an idealized modeling framework. Axisymmetric upper-tropospheric anticyclones are constructed by specifying potential vorticity (PV) and solving the nonlinear PV-inversion problem. The PV distribution has a smooth but near-discontinuous change of PV across the tropopause in a transition zone with vertical depth δ. For fixed δ the strength of the TIL changes with changing resolution until the transition zone is resolved by a fairly large number of grid points. The quality-controlled numerical solutions are used to study the behavior for $\delta \to 0$. This limit can lead to very strong TILs, but no indications for divergent behavior were found.

1. Introduction

The sharpness of the extratropical tropopause has instigated considerable scientific interest in recent years. At the origin of these activities was a paper by Birner et al. (2002), who investigated small-scale climatological features of the tropopause region above Germany using high-resolution radiosonde data. Their analysis was based on an averaging technique that considers the thermal tropopause as a common reference level. The results showed that the mean profiles of buoyancy frequency squared, N^2, have a sharp peak just above the tropopause corresponding to a strong thermal inversion in that region. This layer is now often referred to as the tropopause inversion layer (TIL). The layer of enhanced N^2 is between 500 and 3000 m thick and has characteristic variations with latitude and season. Subsequent analysis by Birner (2006) and Randel et al. (2007) suggested that this feature is characteristic for the entire extratropics.

The physical mechanisms underlying the observed TIL are not well understood. Modeling studies such as those of Wirth and Szabo (2007) or Son and Polvani (2007) suggest that its formation may be due to conservative dry dynamics. Alternatively, Randel et al. (2007) argued that radiative effects associated with water vapor and ozone should play an important role. Further potentially important mechanisms involve gravity waves, turbulence, deep convection, and the Brewer–Dobson circulation. The degree to which any of these processes is relevant in a climatological sense is unknown.

Numerical models have so far not been able to feature a TIL that is as sharp as observed (see also Birner et al. 2006). Clearly there is an issue related to vertical resolution, which is much coarser in these models compared to the 50-m resolution of radiosonde data. In addition, the dependence of the results on horizontal and vertical resolution seems difficult to interpret even in a qualitative sense (Son and Polvani 2007).

This state of affairs motivated us to revisit the problem and systematically investigate the dependence of the TIL on numerical resolution. Our framework is the same idealized model setup as in Wirth (2001, 2003). Idealized axisymmetric vortices are obtained through specifying a potential vorticity (PV) distribution. The latter is designed to imply anomaly generation from a large-scale reference atmosphere through conservative dynamics. Subsequently, PV is inverted for the wind and temperature (Hoskins et al. 1985), which allows one to compute profiles of N^2. The resulting anticyclones are characterized by a sharp peak in N^2 right above the tropopause in the vortex center, whereas the cyclones

Corresponding author address: Andreas Müller, Institute for Atmospheric Physics, University of Mainz, Becherweg 21, 55099 Mainz, Germany.
E-mail: andrmue@uni-mainz.de

DOI: 10.1175/2009JAS3109.1

show a smooth transition of N^2 across the tropopause from tropospheric to stratospheric values. As shown later by Wirth (2004), these features are due to the convergence of the vertical wind, which is part of the implied secondary circulation but which is somewhat hidden in a PV-based approach.

In this note we restrict our attention to anticyclones because we are interested in sharp features of N^2 and their numerical representation. Our reference atmosphere is characterized by piecewise constant values of N^2 (a low value, N_T^2, for the troposphere and a larger value, N_S^2, for the stratosphere), with a smooth transition over a vertical distance δ. The interest in a near-discontinuous reference atmosphere comes from the numerical solutions of Wirth (2003), which suggested an increase of the peak amplitude of N^2 by a fixed value each time when halving δ (see his Fig. 14). If such a logarithmic divergence holds true, it may be a potentially important mechanism possibly contributing to the observed climatology. However, it remained completely open from Wirth (2003) whether the logarithmic divergence is real or simply an artifact of the limited range of resolutions tested.

Thus, we were motivated to reconsider this highly nonlinear PV-inversion problem, but this time with much higher numerical resolution and taking great care to control and limit the numerical error. Our main goals are (i) to study the numerical convergence of the solutions for fixed δ and (ii) to investigate the behavior of the (numerically converged) solutions in the limit $\delta \to 0$. We shall see that a reference atmosphere with a near-discontinuity in N^2 can produce very large peaks in N^2 but that this requires a vertical resolution significantly higher than anything that has been used so far in numerical studies.

2. A model for upper-tropospheric anticyclones

We consider axisymmetric hydrostatic flow of a stably stratified atmosphere on the f plane. Radius is denoted by r and log-p altitude is defined as $z = -\ln(p/p_0)$, where p is pressure, $p_0 = 1000$ hPa is a constant reference pressure, and $H = 7$ km denotes a constant scale height. Potential temperature is given by $\theta = T\exp(\kappa z/H)$, where T = temperature, $\kappa = R/c_p = 2/7$, $R = 287$ J kg^{-1} K^{-1} = gas constant for dry air, and c_p = specific heat at constant pressure). As a natural expression for the buoyancy frequency squared we use

$$N^2(r,z) = \frac{g}{T_s}\left(\frac{\partial T}{\partial z} + \frac{\kappa T}{H}\right) = \frac{g}{T_s}\frac{T}{\theta}\frac{\partial \theta}{\partial z} \qquad (1)$$

(see Andrews et al. 1987), where $g = 9.81$ m s^{-1} is the acceleration due to gravity and $T_s = gH/R$. Using θ as vertical coordinate, this becomes

$$N^2(r,\theta) = \frac{gp^{\kappa+1}}{T_s p_0^{\kappa} H}\left(-\frac{\partial p}{\partial \theta}\right)^{-1}. \qquad (2)$$

Potential vorticity can be written as

$$Q(r,\theta) = \left(f + \frac{\partial(rv)}{r\partial r}\right)\left(-\frac{1}{g}\frac{\partial p}{\partial \theta}\right)^{-1} \qquad (3)$$

(Andrews et al. 1987), where f is the Coriolis parameter and v denotes the tangential wind. Assuming gradient wind balance, the thermal wind equation becomes

$$\left(f + 2\frac{v}{r}\right)\frac{\partial v}{\partial \theta} = R\frac{p^{\kappa-1}}{p_0^{\kappa}}\frac{\partial p}{\partial r} \qquad (4)$$

(e.g., Hoskins et al. 1985).

Our model domain is rectangular extending from 0 to $r_{\max}$ in the radial direction and from $\theta_{\min}$ to $\theta_{\max}$ in the vertical.

First we construct a reference atmosphere that only depends on the vertical coordinate. Its static stability N^2_{ref} is assumed to be piecewise constant with a smooth transition between the tropospheric value $N_T^2 = 10^{-4}\,\mathrm{s}^{-2}$ and the stratospheric value $N_S^2 = 4\times 10^{-4}\,\mathrm{s}^{-2}$. The transition occurs over a vertical depth δ. More specifically, we set

$$N^2_{\mathrm{ref}}(\theta) = (N_S^2 - N_T^2)\mu\left(\frac{\theta - \theta_{\mathrm{TP}}}{\delta} + \frac{1}{2}\right) + N_T^2, \qquad (5)$$

with

$$\mu(x) := \begin{cases} 0, & \text{if } x < 0, \\ (3-2x)x^2, & \text{if } x \in (0,1), \\ 1, & \text{if } x > 1, \end{cases} \qquad (6)$$

and with $\theta_{\mathrm{TP}} = 320$ K denoting the potential temperature of the reference tropopause. Given $N^2_{\mathrm{ref}}(\theta)$, the corresponding pressure distribution $p_{\mathrm{ref}}(\theta)$ is obtained by integrating (2) with $p_{\mathrm{ref}}(\theta = 285\ \mathrm{K}) = 1000$ hPa. Inserting $p_{\mathrm{ref}}(\theta)$ into (3) and setting $v = 0$ yields the potential vorticity $Q_{\mathrm{ref}}(\theta)$. Owing to the near-discontinuous nature of N^2_{ref}, there is a corresponding near-discontinuity in $Q_{\mathrm{ref}}(\theta)$ across the tropopause.

Axisymmetric anomalies are defined by specifying a nominal tropopause potential temperature as follows:

$$\theta_{\mathrm{TP}}(r) = \theta_{\mathrm{TP}} + A\sin^2\left(\frac{\pi}{2}\frac{R_A - r}{R_A}\right). \qquad (7)$$

Key parameters are the amplitude A and the radial extent R_A of the anomaly. The function $\theta_{\mathrm{TP}}(r)$ is used for a smooth transformation of the PV distribution, which modifies PV in the tropopause region but leaves PV

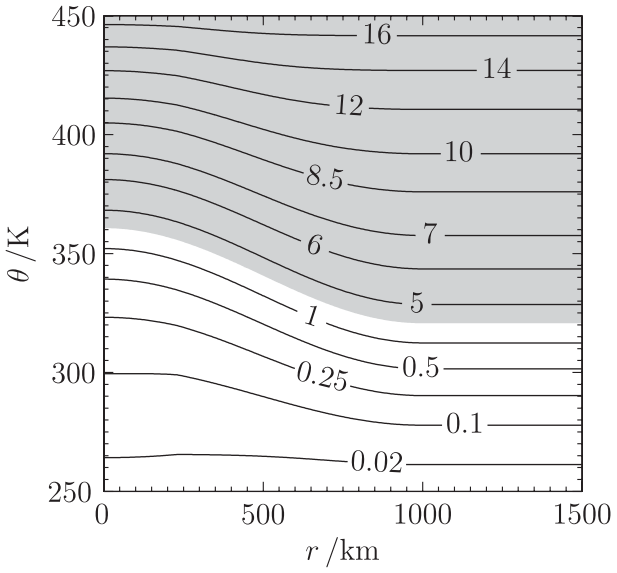

FIG. 1. Specified distribution of potential vorticity $Q(r, \theta)$ (PVU); gray shading indicates $Q \geq 3$ PVU) for $A = 40$ K and $\delta = 20$ K. For reasons of illustration, this figure uses a very large amplitude to convey the transformation as clearly as possible; the transformation is much smoother with typical amplitudes used in this paper.

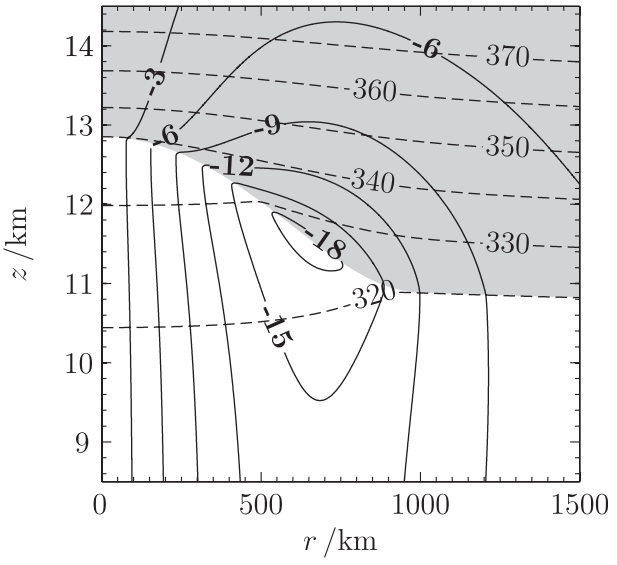

FIG. 2. Tangential wind v (solid, m s^{-1}) and potential temperature θ (dashed, K) as a function of radius r and height z. Gray shading indicates $Q \geq 3$ PVU. The other parameters are $A = 20$ K, $\delta = 2$ K, and $R_A = 1000$ km.

nearly unchanged otherwise (see Fig. 1 for illustration). The details of the transformation are given in the appendix. As was argued in Wirth (2003), such a construction effectively represents anomaly formation through conservative advection of subtropical air and an ensuing cutoff process.

Given the PV distribution $Q(r, \theta)$, tangential wind v and pressure p are obtained through PV inversion (Hoskins et al. 1985). In our case this requires the numerical solution of two coupled nonlinear differential Eqs. (3) and (4). Finally, N^2 is obtained from (2), and the results are transformed to $\log p$ coordinate to facilitate comparison with previous results. As illustrated in Fig. 2, our anticyclones are qualitatively very similar to the warm core upper anticyclones of Thorpe (1986, his Fig. 2).

A key parameter in this study is the maximum value $N^2_{\max}$ of the static stability profile at the center of the anomaly. As a measure for the strength of the TIL we shall consider $N^2_{\max} - N^2_S$. The size of the domain is given through $r_{\max} = 1.5R_A$, $\theta_{\min} = 230$ K, and $\theta_{\max} = 480$ K. Tests showed that this is a good compromise between computational effort and insensitivity of the results with respect to the boundaries, as long as δ is much smaller than the vertical extent of the domain.

3. Numerical solution

Similar to Wirth (2003), the PV inversion is performed through an iterative algorithm following Hoskins et al. (1985). Differentiating (3) with respect to r and replacing $\partial p/\partial r$ through (4) yields

$$\frac{\partial}{\partial r}\left(\frac{\partial(rv)}{r\partial r}\right) + \frac{Q}{g}\frac{\partial}{\partial\theta}\left(h\frac{\partial v}{\partial\theta}\right) = -\frac{1}{g}\frac{\partial p}{\partial\theta}\frac{\partial Q}{\partial r}, \qquad (8)$$

where h is defined as

$$h(r, \theta) := \frac{f + 2v/r}{R p_0^{-\kappa} p^{\kappa-1}}. \qquad (9)$$

The iteration is initialized by assuming that h and p in (8) are given by the reference atmosphere. This renders (8) a linear elliptic PDE for v. It is discretized using centered finite differences with grid increments Δr and $\Delta\theta$. The resulting linear system of equations is solved with the MATLAB standard function "mldivide." Next, we insert the new v into (4) to obtain a new approximation for p by inward integration assuming $p(r_{\max}, \theta) = p_{\text{ref}}(\theta)$ for all θ. This provides a new approximation for h through (9). The updated values for p and h are used in the ensuing solution of (8). The iteration is continued until the maximum change in pressure between two iteration steps is smaller than 0.1 Pa.

The numerical error is estimated on the level of potential vorticity. We compute an a posteriori field Q_{num} by inserting the solutions for p and v into (3). This is compared with the original PV field Q, which was specified a priori. We use two error estimates: ΔQ_{RMS}, which is the root-mean-square of $|Q - Q_{\text{num}}|$, and $\Delta Q_{\max}$,

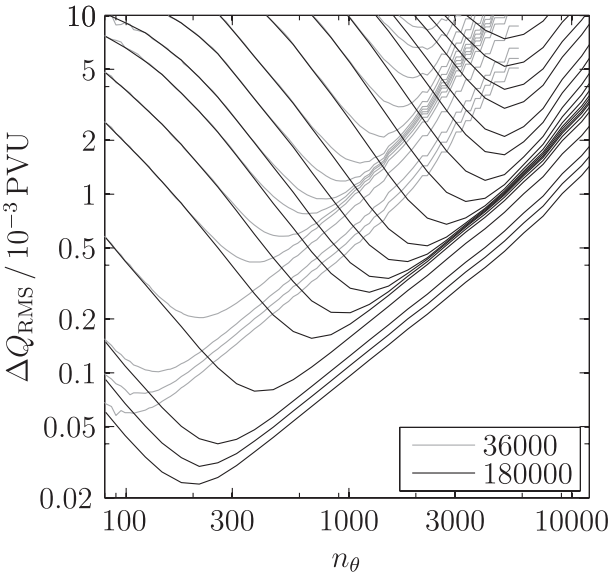

FIG. 3. Error estimate ΔQ_{RMS} as a function of the number n_θ of grid points in the vertical direction for two different resolutions and different values for δ. From bottom to top, δ has the values 100, 85, 70, 40, 20, 14, 10, 8, 6, 4.5, 3, 2, 1.4, 1, 0.8, 0.6, 0.5, 0.4, and 0.3 K, respectively. The legend gives the total number of grid points. The other parameters are $A = 10$ K and $R_A = 1000$ km.

which is the maximum of $|Q - Q_{\mathrm{num}}|$. In both cases only grid points at $r = 0$ are taken into account, since in our analysis we shall focus on the vortex center where we expect the peak in N^2 to be maximum. The error estimates will be given in PV units (PVU) where 1 PVU = 10^{-6} m^2 K s^{-1} kg^{-1}.

By repeating this procedure for different vertical and horizontal grid increments, we found that even for a fixed total number of grid points the numerical error strongly depends on the ratio between the number of grid points in the horizontal and vertical direction. Obviously, the total number of grid points is limited by computational resources. Therefore, much effort was expended to find the optimum choice of horizontal versus vertical resolution for a fixed total number of grid points. Figure 3 shows that this optimum depends both on the transition depth δ and on the total number of grid points. Furthermore, we found that it also depends on the amplitude A and radial scale R_A. Of course, the total number of grid points should be as high as possible. This renders it impractical to determine the optimum value of n_θ for each possible combination of parameters. Fortunately, the low-resolution results suggest systematic dependencies, which allowed us to estimate the optimum n_θ. We tested these dependencies for each resolution used in this work and found that the minimum error is always found very reliably. All results shown in this note are based on this optimization for allotting

TABLE 1. Vertical resolution at the tropopause for the different amplitudes when using a total number of 4.5×10^6 grid points. The other parameters are $\delta = 1$ K and $R_A = 1000$ km.

A (K)	1	2.5	5	10	20
Δz (m)	1.2	1.5	1.7	1.7	1.4

vertical and horizontal resolution for a given total resolution. Table 1 gives the vertical resolution in meters at the tropopause for the different amplitudes when using a total number of 4.5×10^6 grid points.

4. Results

a. Synoptic scale

First we consider an anomaly with a radial scale $R_A = 1000$ km, which is considered typical for synoptic scales. Figure 4 shows $\Delta Q_{\max}$ as a function of the transition depth δ at fixed amplitude $A = 5$ K (a similar behavior was found for other amplitudes and for the error estimate ΔQ_{RMS}). The four different lines correspond to four different values of the total number of grid points, differing by a factor of 5 from each other. The figure indicates that for a given δ the numerical error decreases with increasing total number of grid points. This suggests numerical convergence. Figure 4 also shows that for a given total number of grid points the numerical error increases with decreasing δ. This is not surprising because the gradients in Q and N^2 become steeper for decreasing δ.

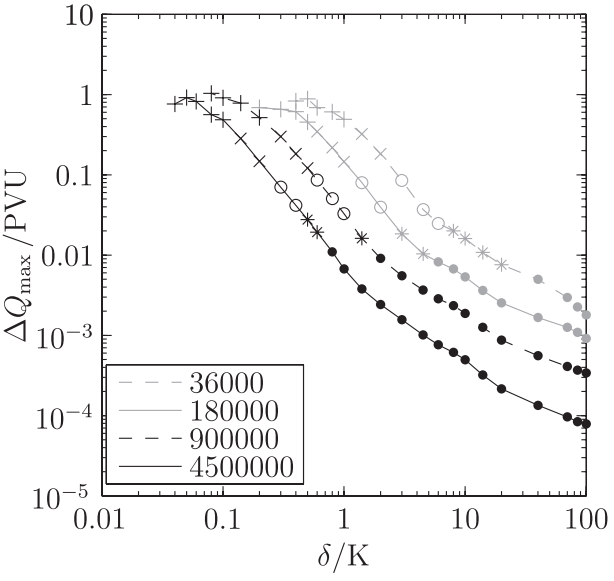

FIG. 4. Error estimate $\Delta Q_{\max}$ as a function of the transition depth δ for different resolutions. The legend gives the total number of grid points. The other parameters are $A = 5$ K and $R_A = 1000$ km. Data points symbols are as follows: + indicates $1 \le \delta/\Delta\theta < 5$; × indicates $5 \le \delta/\Delta\theta < 10$; ○ indicates $10 \le \delta/\Delta\theta < 20$; * indicates $20 \le \delta/\Delta\theta < 30$, and • indicates $\delta/\Delta\theta \ge 30$.

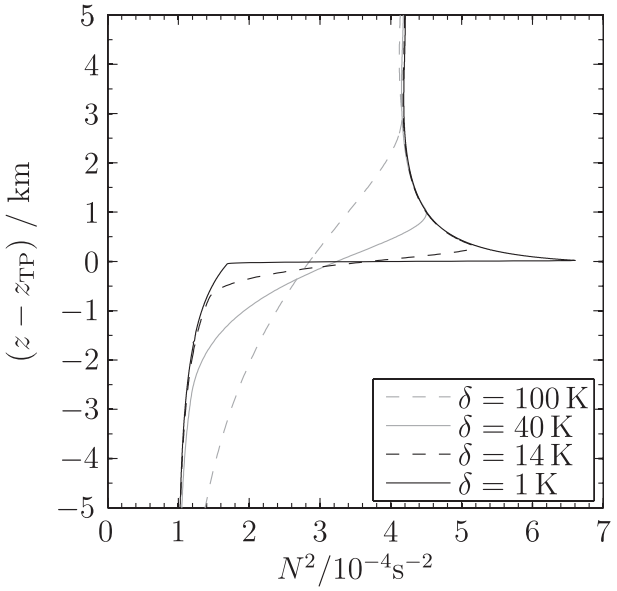

FIG. 5. Profiles of buoyancy frequency squared N^2 in the center of the anomaly for different values of δ as a function of height z relative to the height z_{TP} of the tropopause. The amplitude of the anomaly is $A = 10$ K and the radius is $R_A = 1000$ km.

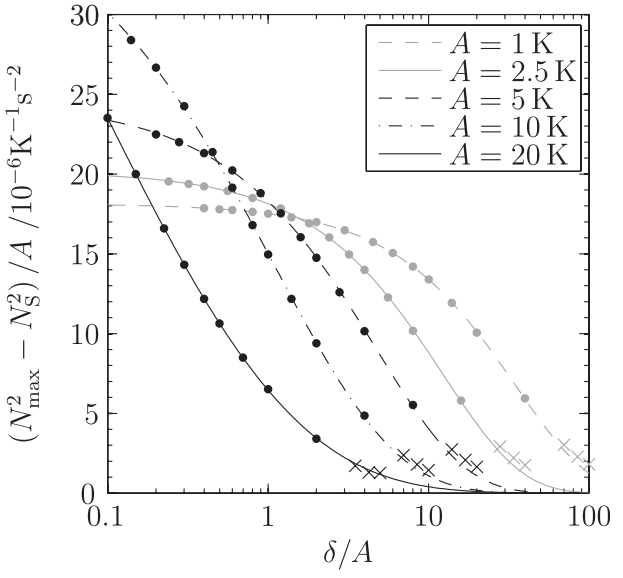

FIG. 6. Normalized TIL strength $(N^2_{max} - N^2_S)/A$ as a function of δ/A for different amplitudes A. The data points represent numerical results (all of them satisfying $\Delta Q_{max} < 0.01$ PVU); the lines are an exponential fit. Data points marked $\times$ are not used for the fit because those large values of δ may be distorted owing to boundary effects in a finite computational domain.

We have to decide what error we can tolerate for the remaining analysis. One reasonable choice would be to take only those values for which the relative error is smaller than 1%. Because the value of the PV near the tropopause is always greater than 1 PVU, this condition implies that ΔQ_{max} must be smaller than 0.01 PVU. The disadvantage is that this condition is a posteriori (i.e., it can be checked only after one has done the calculation). We found a way around this dilemma. The data points plotted with a "•" in Fig. 4 show that the condition $\Delta Q_{max} < 0.01$ PVU agrees very well with the condition

$$\delta > 30\Delta\theta, \tag{10}$$

where $\Delta\theta$ is the vertical grid increment. Similarly, we would get $\delta > 20\Delta\theta$ for a relative error of 3% or $\delta > 10\Delta\theta$ for a relative error of 10%. Overall, we come to the conclusion that the relation (10) is the best compromise between a fairly small error and tolerable computational effort. The main advantage of condition (10) compared to $\Delta Q_{max} < 0.01$ PVU is that it is a priori and allows us to determine the smallest δ down to which we can trust the results for a given resolution $\Delta\theta$. We found that (10) applies to all amplitudes, resolutions, and horizontal scales R_A. Alternatively, (10) allows one to determine the resolution (and thus the computational resources) necessary to obtain reliable results for a given δ. In the remainder of this note we only use numerical results that satisfy the quality criterion (10).

The question remains whether the numerical error in N^2, too, is smaller than 1% when condition (10) is satisfied. Almost all of our results suggest a geometric series convergence. Furthermore, as long as condition (10) is satisfied the variation of $N^2_{max} - N^2_S$ between the different resolutions is always on the order of 1% (or even smaller). This indicates that the restriction of the error in Q carries over to a limited error in N^2.

Figure 5 shows profiles of N^2 for different values of δ. As in Wirth (2003), the profiles of N^2 show a sharp peak just above the tropopause for moderate and small δ. However, it is by no means clear from this figure whether or not the results converge for $\delta \to \theta$.

We investigate this limit in more detail in Fig. 6, which shows N^2_{max} as a function of δ. Note that in this figure the variables on the ordinate have been divided by the amplitude A, which turns out to be beneficial for representing the results for different amplitudes in a single plot. Interestingly, over a limited range of values of δ the strength of the peak (as measured by $N^2_{max} - N^2_S$) increases logarithmically with decreasing δ, consistent with the impression gained from Fig. 5. However, this logarithmic divergence does not apply at smaller values of δ. Indeed, the results for each amplitude can be fitted very well by an exponential function of the form $g(x) = ae^{-(x/x_0)^b}$ (where $x = \delta\mathrm{K}^{-1}$ and where the parameters a, b, and x_0 are determined individually for each amplitude). This strongly suggests that $N^2_{max} - N^2_S$

TABLE 2. Limiting values of $N^2_{\max} - N^2_S$ for $\delta \to 0$ at $r = 0$. These values were obtained by extrapolating the fits shown in Fig. 6.

A (K)	1	2.5	5	10	20
$N^2_{\max} - N^2_S$ (at $r = 0$, in $10^{-4}\,\mathrm{s}^{-2}$)	0.2	0.5	1.2	3.9	14.5

converges toward a finite value in the limit $\delta \to 0$. From the fit functions we obtain the limiting values shown in Table 2.

b. Sensitivity to the aspect ratio

Up to this point we restricted our presentation to anomalies with $R_A = 1000$ km, representing a typical synoptic scale. Care has to be exercised when generalizing results from PV inversion to other scales because the aspect ratio of the anomaly determines the partitioning of a given PV anomaly into a static stability anomaly and relative vorticity anomaly (see Wirth 2003 and appendix A in Wirth 2000). Here, the aspect ratio is proportional to the vertical displacement of the tropopause in geometric space divided by the horizontal scale of the anomaly. The anomalies studied in section 4a are mostly characterized by a shallow aspect ratio. It would be interesting to see how the results would change if we consider taller aspect ratios. Therefore, we repeated our analysis for $R_A = 100$ km, which results in rather tall aspect ratios even for small anomaly amplitudes.

Figure 7 shows the results (note that in this plot the ordinate is *not* divided by A). For a given intermediate value of δ the strength of the TIL is weaker for the tall anomaly in comparison with the shallow anomaly. On the other hand, at first sight the plot seems to indicate overall a less convergent behavior in the limit $\delta \to 0$. However, the data can be fitted very well to the same exponential function as before, suggesting that $N^2_{\max} - N^2_S$ may well remain finite for $\delta \to 0$. Using these exponential fits we obtain limiting values for $N^2_{\max} - N^2_S$ with an order of magnitude between $10 \times 10^{-4}\,\mathrm{s}^{-2}$ and $30 \times 10^{-4}\,\mathrm{s}^{-2}$. These values are significantly higher than for the flat anomalies analyzed before.

This second set of computations with tall aspect ratio corroborates our main conclusions from section 4a: For a fixed value of δ the numerics converge with increasing resolution, and all our results suggest that $N^2_{\max}$ remains finite in the limit $\delta \to 0$, although it can become very large.

5. Summary and conclusions

We systematically investigated the numerical representation of the TIL in an idealized model for upper-tropospheric anticyclones. Axisymmetric PV distributions were specified through a construction that implies a purely dynamic generation from a large-scale reference atmosphere. The latter, in turn, was characterized by two constant values of N^2 (a smaller one for the troposphere and a larger one for the stratosphere), with a smooth transition over a vertical distance δ. We solved the nonlinear PV-inversion problem with very high spatial resolution and with special care regarding the numerical error. To make the best use of computer memory, we designed a technique that optimally allots numerical resolution to the vertical and horizontal dimensions.

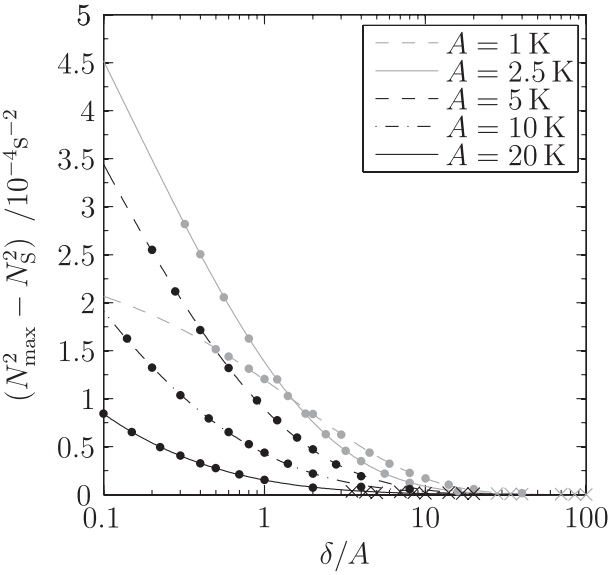

FIG. 7. As in Fig. 6, but for $R_A = 100$ km.

As a key diagnostic we considered $N^2_{\max}$, which is defined as the maximum value of N^2 in the vortex center right above the tropopause. Our results show that the transition region δ must be resolved by approximately 30 grid points to reduce the relative numerical error below 1%. As one might have expected, this result is practically independent of amplitude A of the specified PV anomaly.

In addition, we studied the behavior of the solution for $\delta \to 0$. This limit corresponds to a reference atmosphere with piecewise constant N^2 and a discontinuity in N^2 right at the tropopause. The quality-controlled numerical solutions allowed us to infer a simple exponential dependence of $N^2_{\max}$ as a function of δ for each amplitude A. This was used to extrapolate toward $\delta = 0$. Our results suggest that there is always convergence toward a finite $N^2_{\max}$, although its value may be several times larger than the background stratospheric value. It follows that the apparent logarithmic divergence suggested by Wirth (2003) was due to the limited range of resolutions used in that work. It would be interesting to know whether values as large as in our idealized model can be observed in real anticyclones. If so, the dynamical mechanisms underlying

this work offer an explanation, even though other processes (especially radiation) cannot be excluded a priori.

Overall, we conclude that the dynamical formation of an upper-tropospheric midlatitude anticyclone from a large-scale reference atmosphere with a near-discontinuity in N^2 at the tropopause can yield a TIL with a peak in N^2 several times exceeding typical stratospheric values of N^2. Current mesoscale and global numerical models do not have enough vertical resolution to fully resolve this feature. Such models are, therefore, unlikely to faithfully represent the spatial variability of N^2 within the TIL.

Acknowledgments. We are grateful to W. Paul for stimulating discussions and T. Birner for his insightful comments on an earlier version of this manuscript.

APPENDIX

Specifying a Smooth PV Distribution

We define a modified vertical coordinate $\tilde{\theta}$ through

$$\tilde{\theta} := \theta - A \sin^2\left(\frac{\pi}{2}\frac{R_A - r}{R_A}\right)\Lambda(r,\theta), \tag{11}$$

if $r < R_A$, and $\tilde{\theta} := \theta$ otherwise. This transformation is consistent with (7). The symbol Λ denotes a smooth hat function defined by

$$\Lambda(r,\theta) := \exp\left\langle \gamma(r)\left\{1 - \frac{\alpha_T^2(r)\beta}{\theta - \theta_{\min}} + \frac{[1-\alpha_T(r)]^2\beta}{\theta - \theta_{\max}}\right\}\right\rangle, \tag{12}$$

if $\theta \in (\theta_{\max}, \theta_{\min})$, and $\Lambda(r, \theta) := 0$ otherwise. The functions $\alpha_T(r)$ and $\gamma(r)$ and the constant β were chosen empirically so that the transformation of the PV distribution is as smooth as possible:

$$\alpha_T(r) := \frac{\theta_{\mathrm{TP}}(r) - \theta_{\min}}{\theta_{\max} - \theta_{\min}}, \tag{13}$$

$$\beta := \theta_{\max} - \theta_{\min}, \tag{14}$$

$$\gamma(r) := 5\left|\alpha_T(r) - \frac{1}{2}\right| + 2. \tag{15}$$

The PV distribution is obtained by inverting (11) numerically and setting $Q[r, \theta(r, \tilde{\theta})] = Q_{\mathrm{ref}}(\tilde{\theta})$.

REFERENCES

Andrews, D. G., J. R. Holton, and C. B. Leovy, 1987: *Middle Atmosphere Dynamics*. Academic Press, 489 pp.

Birner, T., 2006: Fine-scale structure of the extratropical tropopause region. *J. Geophys. Res.,* **111,** D04104, doi:10.1029/2005JD006301.

——, A. Dörnbrack, and U. Schumann, 2002: How sharp is the tropopause at midlatitudes? *Geophys. Res. Lett.,* **29,** 1700, doi:10.1029/2002GL015142.

——, D. Sankey, and T. G. Shepherd, 2006: The tropopause inversion layer in models and analyses. *Geophys. Res. Lett.,* **33,** L14804, doi:10.1029/2006GL026549.

Hoskins, B. J., M. E. McIntyre, and A. W. Robertson, 1985: On the use and significance of isentropic potential vorticity maps. *Quart. J. Roy. Meteor. Soc.,* **111,** 877–946.

Randel, W. J., F. Wu, and P. Forster, 2007: The extratropical tropopause inversion layer: Global observations with GPS data, and a radiative forcing mechanism. *J. Atmos. Sci.,* **64,** 4489–4496.

Son, S.-W., and L. M. Polvani, 2007: Dynamical formation of an extra-tropical tropopause inversion layer in a relatively simple general circulation model. *Geophys. Res. Lett.,* **34,** L17806, doi:10.1029/2007GL030564.

Thorpe, A. J., 1986: Synoptic-scale disturbances with circular symmetry. *Mon. Wea. Rev.,* **114,** 1384–1389.

Wirth, V., 2000: Thermal versus dynamical tropopause in upper-tropospheric balanced flow anomalies. *Quart. J. Roy. Meteor. Soc.,* **126,** 299–317.

——, 2001: Cyclone–anticyclone asymmetry concerning the height of the thermal and the dynamical tropopause. *J. Atmos. Sci.,* **58,** 26–37.

——, 2003: Static stability in the extratropical tropopause region. *J. Atmos. Sci.,* **60,** 1395–1409.

——, 2004: A dynamical mechanism for tropopause sharpening. *Meteor. Z.,* **13,** 477–484.

——, and T. Szabo, 2007: Sharpness of the extratropical tropopause in baroclinic life cycle experiments. *Geophys. Res. Lett.,* **34,** L02809, doi:10.1029/2006GL028369.